Dalton Transactions

RSC Publishing

PAPER

Multifunctional iron-chelators with protective roles against neurodegenerative diseases†

Cite this: *Dalton Trans.*, 2013, **42**, 6058

Andreia Nunes,[a] Sérgio M. Marques,[a] Catarina Quintanova,[a] Diana F. Silva,[b] Sandra M. Cardoso,[b,c] Sílvia Chaves[a] and M. Amélia Santos*[a]

Received 8th October 2012,
Accepted 22nd February 2013

DOI: 10.1039/c3dt50406a

www.rsc.org/dalton

The multifactorial nature of Alzheimer's disease (AD), and the absence of a disease modifying drug, makes the development of new multifunctional drugs an attractive therapeutic strategy. Taking into account the hallmarks of AD patient brains, such as low levels of acetylcholine, misfolding of proteins and associated beta-amyloid (Aβ) aggregation, oxidative stress and metal dyshomeostasis, we have developed a series of compounds that merge three different approaches: metal attenuation, anti-Aβ aggregation and anti-acetylcholinesterase activity. Therefore, 3-hydroxy-4-pyridinone (3,4-HP) and benzothiazole molecular moieties were selected as starting frameworks due to their well known affinity for iron and Aβ peptides, respectively. The linkers between these two main functional groups were selected on the basis of virtual screening, so that the final molecule could further inhibit the acetylcholinesterase, responsible for the cholinergic losses. We describe herein the design and synthesis of the new hybrid compounds, followed by the assessment of solution properties, namely iron chelation and anti-oxidant capacity. The compounds were bioassayed for their capacity to inhibit AChE, as well as self- and Zn mediated-$A\beta_{1-42}$ aggregation. Finally, we assessed their effects on the viability of neuronal cells stressed with $A\beta_{42}$.

Introduction

Alzheimer's disease (AD) is a chronic, irreversible and progressive disorder, which is characterized by dementia, cognitive impairment and memory loss and, in an advanced stage, it can lead to incapacitation and finally to death.[1,2] AD etiology is not completely understood, but it is recognized as a multifaceted disorder in which the patients brains show several features such as low levels of acetylcholine, misfolding of proteins and associated aggregation processes, oxidative stress and free radical formation, metal dyshomeostasis, protein phosphorylation impairment as well as mitochondrial and neuroinflammatory dysfunctions. Thus, the complexity of this pathology justifies the absence of effective disease-modifying AD therapeutics.[3,4]

The senile plaques and neurofibrillary tangles are the main hallmarks of AD and result from deposition of a beta-amyloid (Aβ) peptide and τ-protein, respectively. However, the cellular toxicity associated with the aggregation of Aβ fibrils has been considered one of the major justifications for the loss of neuronal cells that occur in AD patients.[5]

Although the mechanism of protein folding and aggregation in neurodegeneration remains unclear, there is plenty of evidence about the role of several factors in that process, such as redox-active metal ions and oxidative stress.[6] In fact, the brain metal concentration seems to increase with age,[7,8] and this metal imbalance can be responsible for two major contributions to the neurodegeneration process: the redox-active metal ions, such as Fe(III) and Cu(II), can be reduced by H_2O_2 and promote the Fenton reaction with the formation of reactive oxygen species (ROS), which may then oxidize biomolecules and induce severe damage in neuronal cells;[9] several metal ions, such as Zn(II), can modify protein structure (misfolding) and lead to abnormal aggregation and formation of beta-amyloid deposits.[10,11] Therefore, the critical role of the metal imbalance in neurodegeneration has made the chelating therapy an attractive strategy to be used against the development and the progression of AD and other neurodegenerative disorders.[12–14]

The dysfunctional Aβ has been the pivotal pharmacological target for AD, but up to now the only approved AD therapy is for improving the symptomatic cognitive deficits through the inhibition of acetylcholinesterase (AChE) (*e.g.* donepezil, tacrine and rivastigmine), although only moderate benefits have been reported.[15] Quite often coadjutant drugs have also

[a]*Centro de Química Estrutural, Instituto Superior Técnico, Universidade Técnica de Lisboa, Av. Rovisco Pais 1, 1049-001 Lisboa, Portugal. E-mail: masantos@ist.utl.pt; Fax: +351-218464455; Tel: +351-218419273*

[b]*Centro de Neurociências e Biologia Celular, Universidade de Coimbra, 3030 Coimbra, Portugal*

[c]*Faculdade de Medicina, Universidade de Coimbra, 3030 Coimbra, Portugal*

†Electronic supplementary information (ESI) available. See DOI: 10.1039/c3dt50406a

been used, including antioxidants (*e.g.* poly-phenolic and chalcone derivatives)[16] and metal-chelators (*e.g.* desferrioxamine and hydroxyquinolines).[13,14,17]

Hence, due to the recognized multi-factorial nature of AD, a new paradigm has arisen to address this pathology, according to which one single molecular entity can hit more than one target (multifunctional drugs). This leads to the development of hybrid compounds with at least two of the following properties: cholinergic, antioxidant, metal attenuator, Aβ reductor.[18,19]

Based on the same assumption, we have decided to develop and study a new series of compounds that will merge different pharmacological targets, as prospective drug candidates for AD treatment. Specifically, in this paper we combine metal-attenuation and anti-oxidant activity with anti-Aβ aggregation/vectorization roles, as well as a potential cholinergic effect.

As metal-attenuators, 3-hydroxy-4-pyridinones (3,4-HP) are proposed, due to their "privileged" properties for medicinal metal related drugs, namely their high affinity for iron (but low affinity for common biological electrolyte ions), anti-oxidant properties and low toxicity (*e.g.* deferiprone, DFP, is a current iron-chelating drug, see Fig. 1).[20] The extrafunctionalization with benzothiazole (BTA), as a thioflavin-T (ThT) derivative, is based on its known strong affinity for amyloid fibrils and use in Aβ imaging probes.[21] Recent reports have also proposed a new therapeutic strategy against neurodegenerative diseases, based on using chemical agents capable of disrupting metal–peptide interactions which are believed to induce the Aβ aggregation. The correlation between metal ions and amyloid plaques has been investigated, including the role of metals in promoting Aβ aggregation and the formation of ROS, and consequently oxidative stress.[22,23] Very recently, a few hybrid compounds with metal-chelating and amyloidophilicity properties have been reported.[14,24,25] For this new series of potential AD hybrid drugs, the main moieties (3,4-HP and BTA) were connected with a linker, which was modeled by *in silico* tools in order to best provide AChE inhibitory capacity.

In summary, herein we describe the design of these BTA–HP polyfunctional compounds, the synthetic procedure, the evaluation of their solution properties (acid–base, iron complexation, anti-oxidant) and biological properties, such as the assessment of their capacity for inhibition of AChE and of self- and zinc-mediated-Aβ aggregation, as well as their ability to rescue neuronal cells stressed with Aβ, in the absence/presence of iron/ascorbate.

Results and discussion

Molecular modeling

The strategy followed for the design of the new inhibitors consisted of making a pre-selection of several connecting groups (spacers) between the two main moieties, the hydroxypyridinone (HP) and the benzothiazole (BTA) (Fig. 1), and then performing the virtual screening of these molecules against a target enzyme (AChE). The spacer groups tested derived from a combination of amino acid precursors that vary in length, lipophilic character as well as number and position of H-donating capabilities.

Analysis of the crystallographic structures of AChE showed that the catalytic centre of the enzyme is found in the bottom of a deep and narrow gorge that spreads for ~20 Å and is lined by 14 aromatic residues with functional roles, which are conserved between the different species. The active center is composed of three main areas: the catalytic center, which is found in the bottom of the gorge, consists of the catalytic triad: Ser200, His440 and Glu327. Here is where the hydrolysis of the ester bond of acetylcholine (ACh) occurs. The catalytic active site (CAS), located in the proximities of the catalytic triad, is composed of two aromatic residues, Trp84 and Phe330; the

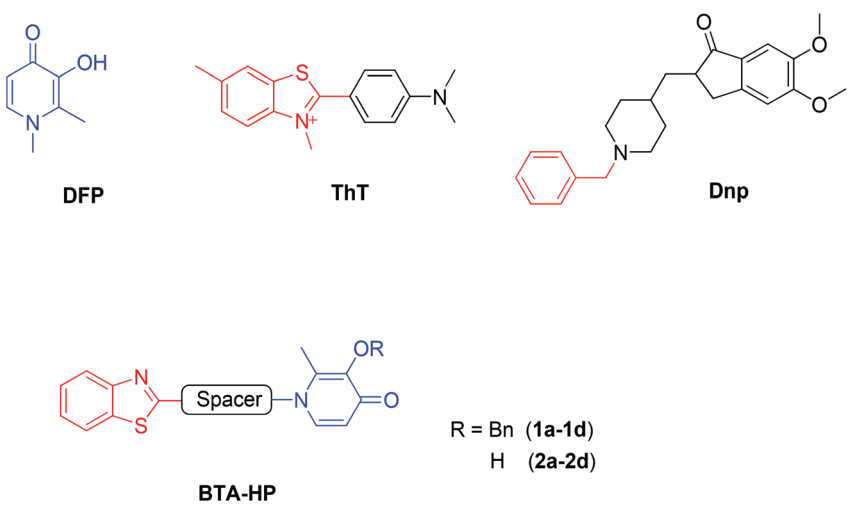

Fig. 1 Deferiprone (DFP), thioflavin-T (ThT), donepezil (Dnp) and schematic representation of the new benzothiazole–hydroxypyridinone (BTA–HP) hybrid compounds.

peripheral active site (PAS), which is located at the entrance of the gorge, presents also two aromatic residues, Tyr70 and Trp279.[26–29] It has been proven that the PAS of the AChE can promote aggregation and deposition of the Aβ peptides. This discovery has stimulated a great interest in a strategy of bivalent ligands that can simultaneously inhibit the hydrolysis of ACh and the aggregation of Aβ induced by AChE.[26,27]

The docking calculations were performed with GOLD software,[30] using as a receptor an X-ray structure of the AChE, *Torpedo californica* variant (TcAChE), complexed with donepezil (Dnp), which was taken from the RCSB Protein Data Bank (PDB, entry code 1EVE).[31] Dnp has some structural parallelism with our compounds in terms of enzyme interaction features (the BTA is expected to occupy the position of the benzyl group of Dnp). This fact ensures a higher proximity of the position of the amino acid side chains in the model structure with respect to our case.

In Fig. 2 are displayed the compounds which presented the best results from the docking. Series **1** corresponds to the *O*-benzyl protected analogues of series **2** compounds, which are in fact the target BTA–HP hybrid multifunctional compounds. Those compounds presented, in general, higher affinities for binding the AChE enzyme than the free HP analogues (series **2a–2d**). This fact is attributed to the strong lipophilic character of the AChE catalytic gorge, which consequently interacts better with the more hydrophobic compounds **1**. The hydroxyl protection of these compounds with a benzyl group also might have a positive contribution by enhancing the blood–brain barrier (BBB) crossing ability. To some extent, the *O*-benzylated compounds may modulate the corresponding *O*-carbamate derivatives which can be considered as prodrugs.

The highest docking scores were obtained for **1a**, **1b** and **2c** (see Table S1 in ESI†). It was observed that these compounds can be well inserted into the active site, maintaining several of the aromatic interactions established by the reference inhibitor, Dnp (see Fig. 3a and Fig. S1, ESI†). The *O*-substituent benzyl group in **1a** forms π–π stacking with the Trp84 residue of the CAS, while the BTA–CH_2–Ph-system may form aromatic interactions at the more external part of the catalytic site, namely with PAS (Tyr70 and Trp279 residues), and a weak H-bond between the BTA sulfur atom and the Tyr70 OH group. Also some aromatic interactions between the pyridinic ring of HP and Phe330 can be formed, although to a lesser extent. The conformation adopted by **1b** is not very different from **1a**, only slightly distorted within the gorge. Regarding the HP–OH analogues, their conformation can be quite different. Analysis of the docking conformation obtained with **2a** (analogue of **1a**) shows that the BTA group "takes" the place of the benzyl group of the previous compounds at the CAS, forming π–π stacking with the Trp84 residue, whereas the adjacent phenyl ring seems to highly interact with the Tyr334 phenol ring (Fig. 3b and Fig. S2†). The HP moiety interacts at the PAS with Trp279, while its OH group is solvent exposed and its carbonyl group may form an H-bond with the Tyr70 OH group. On the other hand, compound **2b** (analogue of **1b**) is docked in the opposite direction. Its HP ring seems to interact at the CAS with Trp84 and the OH and carbonyl groups establish H-bonds with Gly117 carbonyl and Tyr130 OH groups, respectively, while the adjacent phenyl group forms van der Waals contact with the Phe330 aromatic ring. In this case, the BTA group is pointing outside the cavity and forms π–π stacking with Trp279 at the PAS. According to docking, compound **2d** seems to bind AChE in a similar way to **2a**, with its 5-membered ring forming hydrophobic interactions with both Phe330 and Tyr334 residues (Fig. 3c and Fig. S2†).

Chemistry

The synthesis of the BTA–HP compounds involved several steps, including standard protection and activation strategies (see Fig. 4).

The first stage of syntheses consisted of the preparation on the two main molecular moieties, the HP and the BTA. For the HP synthesis, the maltol (3-hydroxy-2-methyl-4-pyrone) was first protected with a benzyl group to avoid side reactions with the hydroxyl group in the subsequent steps. The second step corresponded to a Michael reaction between the *O*-benzyl

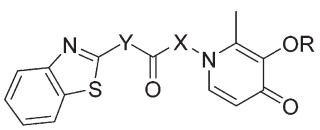

BTA-HP

1a-1d (R = Bn)

2a-2d (R = H)

Group \ Series	a	b	c	d
X	-$(CH_2)_3$-	-CH_2- 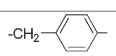	-CH_2- 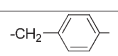	-$(CH_2)_3$-
Y	-CH_2- 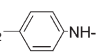 -NH-	-CH_2- 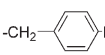 -NH-	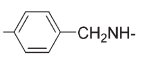 -CH_2NH-	

Fig. 2 General formula of the hybrid benzothiazole–hydroxypyridinone (BTA–HP) chelators (**2a–2d**), and corresponding benzyl derivatives (**1a–1d**), with the list of the linkers selected from *in silico* design.

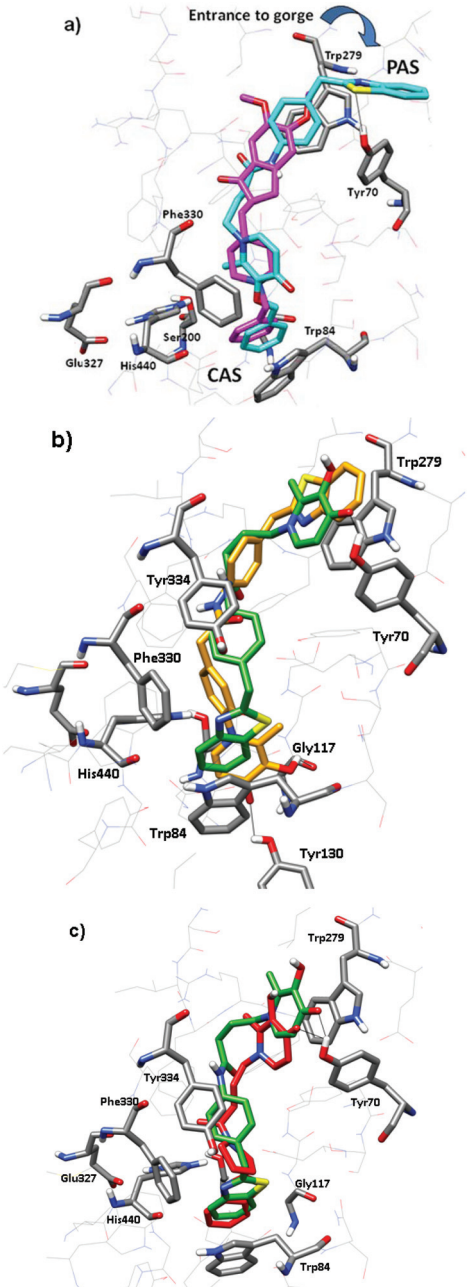

Fig. 3 Docking results for some BTA–HP derivatives with AChE: (a) superimposition of **1a** (cyan) with Dnp (magenta); (b) **2a** (green) and **2b** (yellow); (c) **2a** (green) and **2d** (red). H-bonds are represented as solid black lines.

protected pyrone, **3**, and the suitable aminocarboxylic acids to obtain compounds **4**. These intermediates can be directly coupled with the BTA derivatives (compounds **5**) to afford compounds **1**, or they can be subjected to a prior deprotection to give compounds **6** and subsequently compounds **2**. For deprotection of the hydroxyl group, a standard hydrogenolysis procedure was used (1.5 bar H_2 with Pd/C as a catalyst).

Regarding the benzothiazole derivatives, **5**, their synthesis involved the condensation of 2-aminothiophenol and different amino acid derivatives in polyphosphoric acid to afford compounds **5a–5c**.

After preparation of the two molecular fragments, the final hybrid compounds (**1** and **2**) were obtained by condensation of the BTA-amine with the HP-carboxylic compounds *via* formation of an amide linkage. The reaction conditions depended on the presence of the benzyl group in the final HP moiety. In the case of the *O*-benzylated compounds (compounds **5**), there is no danger of attack in the HP group, so the coupling reaction involved the use of a current activating agent (EDC·HCl). As regards the unprotected compounds (compounds **6**), the OH group of the HP moiety is prone to be attacked, so there is need of using a protecting group. In this case we were able to do it *in situ* with 2 equivalents of ethylchloroformate (ECF), which acts not only as an activating agent of the carboxylic moiety, but also as a protecting agent for the HP–OH group to form the respective ethyl carbonate. The deprotection of the final product was easily accomplished by hydrolysis with a basic solution. We have tried to prepare compounds **2** by simply hydrogenating the benzyl-analogues, **1**. However, due to the presence of a sulfide group in the BTA moiety, the Pd/C catalyst was poisoned and the hydrogenation could not be accomplished.

Acid–base properties

Four of the developed compounds (**2a–2d**) include a free HP chelating moiety in their structure. Since HPs are well known as strong hard metal ion chelators, these compounds are thought to have an important role in diminishing ROS. Therefore, **2a** and **2d** were chosen as models to confirm the high iron chelating ability of these compounds and the results are herein compared to those obtained for DFP (1,2-dimethyl-3-hydroxy-4-pyridinone, DMHP, see Fig. 1) under the same experimental conditions. In order to study the iron chelating ability, the acid–base behavior of the compounds ought to be first analyzed. To improve the solubility of these BTA–HP derivatives, especially **2a**, the solution studies were performed in a mixed DMSO–H_2O medium (50% w/w). Nevertheless, in terms of cellular studies, the final concentration of DMSO used in culture media did not exceed 0.05% (v/v) and no alterations were observed in cells.

To use lower ligand concentrations, spectroscopic protonation titrations were performed instead of potentiometric ones. The stepwise protonation constants were obtained by fitting analysis of the spectrophotometric data with the PSEQUAD program[32] and the values are included in Table 1.

Compounds **2a** and **2d** were isolated in the neutral form (HL) but both have two dissociable protons (H_2L^+). The protonation equilibria for this set of unprotected BTA–HP compounds are shown in Scheme 1, where the first protonation constant (K_1) corresponds to the protonation of the 3-hydroxy whereas the second one (K_2) is attributed to the 4-hydroxy-(*N*-pyridinyl) groups, as found for DFP.

Table 1 shows that the obtained log K_i values are in accordance with those determined herein in the same solvent mixture for DFP. The log K_2 value obtained in water for DFP is also similar to the values achieved in the solvent mixture although the log K_1 value is lower in water (9.77) than in the

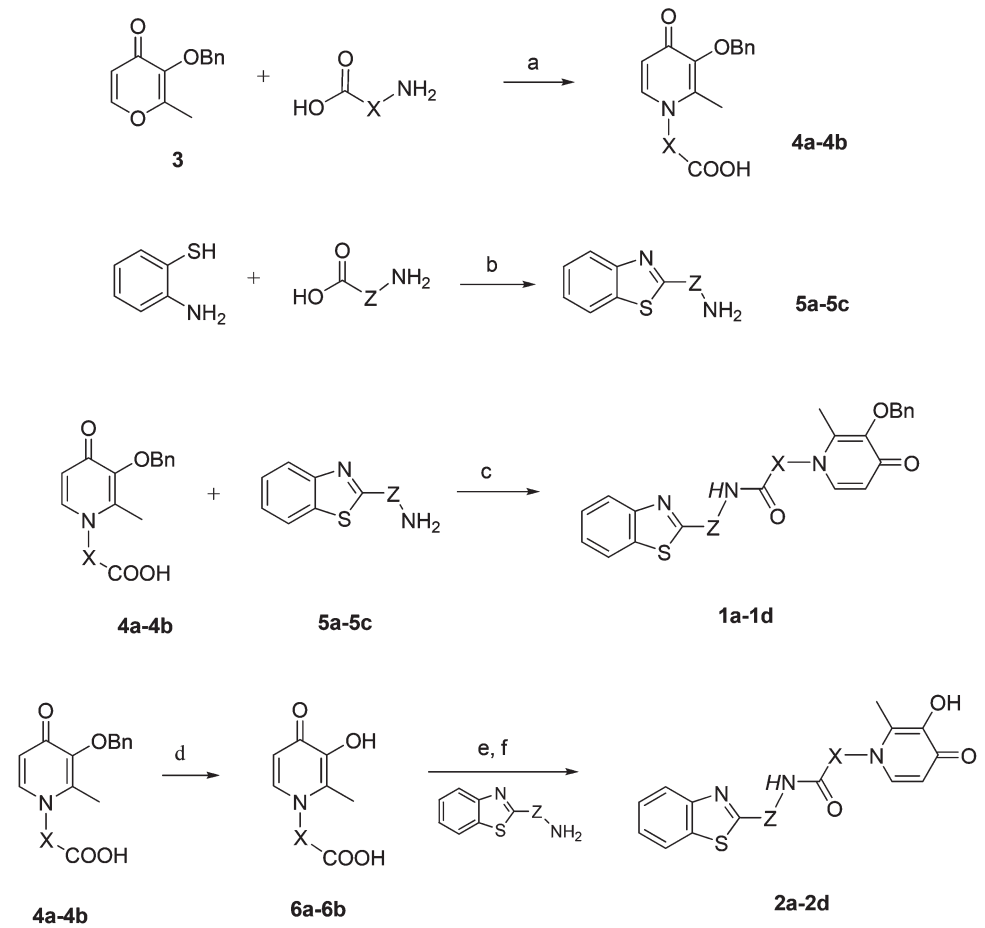

Fig. 4 Reagents and conditions: (a) 10% NaOH, MeOH, reflux or 0.1 M HCl–EtOH, reflux; (b) polyphosphoric acid, 220 °C; (c) EDC·HCl, DMAP, CH_2Cl_2, rt; (d) 10% Pd/C, MeOH, H_2, rt; (e) ECF, NMM, dry CH_2Cl_2; (f) 2% $NaHCO_3$–EtOH, 65 °C. For simplification, we defined Z as the carbon chain of Y, where X and Y are the same substituents as in Fig. 2. In compounds **1d** and **2d** Z is cyclic, and therefore, in this case, "ZN*H*" has no H-atom attached to ZN.

Table 1 Stepwise protonation constants (log K_i) of **2a**, **2d** and DFP as well as the global formation constants of their Fe(III) complexes (I = 0.1 M KCl, 50% DMSO–H_2O, T = 25.0 ± 0.1 °C)

Compound	**2a**	**2d**	**DFP**
log K_1	10.38(4)	10.55(1)	10.77(1) 9.77[a]
log K_2	3.69(8)	3.42(3)	3.51(3) 3.62[a]
log β_{FeL}	16.67(7)	16.00(6)	16.26(5) 15.14[a]
log β_{FeL_2}	29.02(2)	28.80(2)	29.86(2) 26.68[a]
log β_{FeL_3}	37.71(4)	38.08(4)	40.39(3) 35.92[a]
pFe[b]	**19.4**	**19.2**	**20.8**
log P			−0.85

[a] Ref. 33 (I = 0.1 M KCl, T = 25.0 °C, in water). [b] pFe values at pH = 7.4 ($C_{Fe} = 10^{-6}$ M, C_L/C_{Fe} = 10).

50% w/w DMSO–H_2O medium (10.4–10.6), which is according to the Born electrostatic solvent effect.[34]

As a representative example, Fig. S3† shows the electronic spectra and species distribution curves relative to the protonation of **2d**. From this figure, it is clear that for 5.5 < pH < 8.0, 100% of the neutral HL species is present, while for pH above 10.6 the predominant species is totally deprotonated (L^-).

Iron chelating capacity

The complexation abilities of **2a** and **2d** towards iron(III) were evaluated through the determination of the global stability constants of their complexes as well as the pattern of the species distribution curves. Once more, the spectrophotometric method was adopted, instead of the potentiometric one, because at pH 2 a high percent of FeL complex was already formed. The global stability constants (see Table 1) were calculated from the fitting analysis of the measured UV-Vis spectra with the aid of the PSEQUAD program.[32] Firstly, below pH 2, under 1 : 1 M/L stoichiometric ratio conditions, a batch titration was performed in order to determine β_{FeL}; afterwards, for pH > 2, a spectrophotometric titration was performed in a 1 : 3 Fe/L molar ratio and its data analysis (while keeping constant the log β_{FeL} value) allowed the determination of log β_{FeL_2} and log β_{FeL_3}.

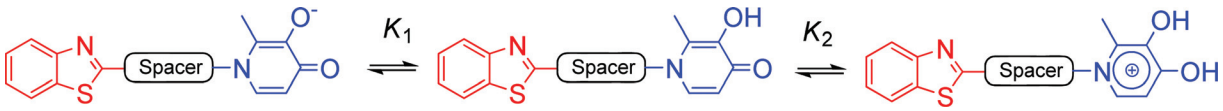

Scheme 1 Protonation equilibria for the unprotected BTA–HP (**2a–2d**) compounds.

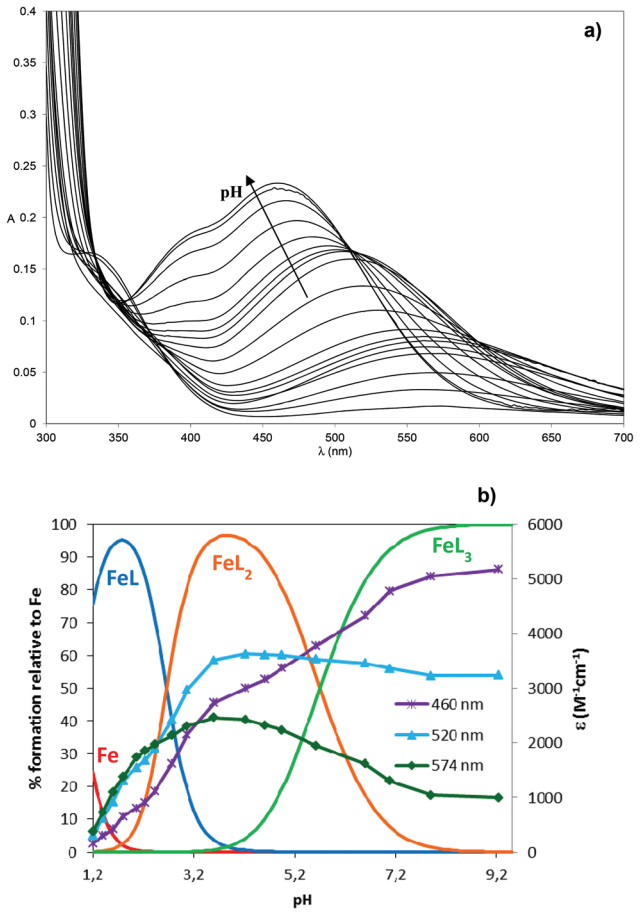

Fig. 5 (a) Electronic spectra (pH 1.2–9.2) and (b) species distribution curves with molar extinction coefficients at maximum absorption wavelengths for the Fe^{3+}/**2d** system (C_L/C_{Fe} = 3.1, C_{Fe} = 4.51 × 10^{-5} M).

Fig. 5 (example for **2d**) evidences the formation of successively stronger complexes, from bis- to hexa-coordinated species, as indicated by the blue shift and the absorbance increase on the metal-to-ligand charge-transfer (CT) band.

Analysis of Fig. 5a shows a clear isosbestic point at *ca.* 510 nm, relative to the interconversion of the bischelated (FeL_2) to the trischelated (FeL_3) species. Moreover, the species distribution curves depicted in Fig. 5b, combined with the absorptivity at 460 and 520 nm, reveal that the maximum absorbance at 460 nm (ε = 5173 M^{-1} cm^{-1}) and 520 nm (ε = 3632 M^{-1} cm^{-1}) corresponds, respectively, to the FeL_3 and FeL_2 CT bands. The observed spectral parameters for the FeL_3 CT band, especially the λ_{max} value, are analogous to those obtained for the CT band of the ferric tris-chelated complex with DFP in 50% w/w DMSO–H_2O (460 nm, 1533 M^{-1} cm^{-1}) or even in water (460 nm, 5800 M^{-1} cm^{-1}).[35] The band with an absorbance maximum at 574 nm should correspond to the monochelated species (FeL). Furthermore, Fig. 5b shows that the main complex formed at pH above 5.7 is the hexacoordinated species (tris-chelate). Analysis of data depicted in Table 1, in particular the pFe values at pH 7.4, evidences that the studied compounds are strong iron chelators, similarly to the oral clinical chelating agent DFP. The high iron(III)-chelating capacity should have an important role in the anti-oxidant activity of the compounds, by preventing the reduction of Fe(III) to Fe(II) and the concomitant hydroxyl radical ($HO^{\cdot}$) formation, as previously reported for DFP (redox behaviour and $HO^{\cdot}$ scavenging activity), which showed to be able to prevent the redox cycling of iron.[36]

Anti-oxidant activity

The new compounds were screened for their anti-oxidant activity (EC_{50}), based on their interaction with the 2,2-diphenyl-1-picrylhydrazyl (DPPH) free radical, and the corresponding results are summarized in Table 2.

Analysis of the results clearly shows that, as expected, the compounds with an *O*-protected HP moiety (compounds **1**) presented much lower anti-oxidant activity (all with EC_{50} > 1 mM) than those with a free hydroxyl group, which is supposed to have an important role in inhibition of the radical formation and also in its capture (compounds **2**).[36] Regarding the unprotected compounds, **2c** appears to be the least anti-oxidant compound (713 μM), although **2a** and **2b** also did not present particularly good EC_{50} values. Among the set of studied compounds, **2d** showed the best anti-oxidant capacity (147 μM), very similar to that of DFP. This appears as a promising result, considering that this compound also presented good AChE inhibitory capacity (see below). The better anti-oxidant activity of **2d** may be explained by the fact that, when compared with the other analogues, this compound does not include any aromatic segment in the spacer between the BTA and HP groups, providing the lowest lipophilic character, which can favor solubility and molecular interactions. These features may contribute to some restriction on the molecular ability to adopt a conformation where the opposite side (BTA group) can make steric hindrance, which may interfere with the interaction between the HP moiety of the compounds and the radical that is to be extinguished.

Pharmacokinetic properties

In order to estimate the potential of the new compounds as eventual drugs, a few indicators of their pharmacokinetic profiles were calculated using the QikProp program.[37] Parameters such as the lipo-hydrophilic character (log *P*), the ability to cross the blood–brain barrier (log *BB*), their ability to be

Table 2 Biological activities of the BTA–HP derivatives (**1** and **2** series), and also the FDA-approved drugs Dnp and DFP, towards radical scavenging (DPPH), inhibition of AChE and $A\beta_{1-42}$ aggregation, as well as some predicted pharmacokinetic parameters

Compd	EC_{50} DPPH[a] (μM)	IC_{50} AChEi[a] (μM)	Anti-Aβ aggreg.[a,b] (%)	clog P[c,d]	log BB[c,e]	Caco-2 permeability (nm s^{-1})[c]
1a	>1000	22.3	45.6	6.75	−1.47	702
1b	>1000	29.2	19.7	7.71	−1.08	1169
1c	>1000	13.8	68.9	6.68	−0.87	1231
1d	>1000	285	47.5	4.46	−0.58	1289
2a	397	>500	—	4.06	−1.93	180
2b	428	>500	—	5.11	−1.54	332
2c	713	>500	—	4.08	−1.28	372
2d	148	14.7	59.3	2.30	−1.04	301
Dnp	—	0.033[f]	—	4.43	0.13	913
DFP	133	—	—	0.62	−0.28	1099

[a] The standard deviation is within 10% of the values. [b] Inhibition of self-mediated Aβ (1–42) aggregation. The thioflavin-T fluorescence method was used, and the measurements were carried out in the presence of an inhibitor (100 μM). [c] Predicted values using the QikProp program, v. 2.5, ref. 37. [d] Calculated octanol–water partition coefficient. [e] Calculated brain–blood partition coefficient. [f] Ref. 38.

absorbed through the intestinal tract to the blood (Caco-2 cell permeability), and the verification of *Lipinski's rule of five* may give an idea of their *druglikeness* for being orally used as anti-AD agents.

As observed from Table 2, **1a–1c** presented the highest predicted octanol–water log P coefficients (clog P), which are >5. They also have molecular weights (MW) > 500, which makes them to have 2 Lipinski's rule violations. This fact, together with the negative log BB (<−1.0 for **1a** and **1b**), does not lead them to be likely good drug candidates, even if they show high Caco-2 permeability rates (>500 nm s^{-1} is considered good). Compound **1d** presents no Lipinski's rule violation, and it has the highest log BB and Caco-2 permeability values of all the new compounds.

Regarding compounds **2**, all except **2b** presented more moderate log P and MW < 500. However, for **2a–2c**, their log BB values are quite low, **2d** having the highest value (−1.0). Considering the Caco-2 permeability, it seems to be moderate (between 180 and 372 nm s^{-1}), and again, compound **2d** displayed a relatively good value (301 nm s^{-1}). Comparatively, the commercial drugs Dnp and DFP showed better pharmacokinetic parameters, namely for their log BB and Caco-2 permeability values.

Altogether, these results suggested **1d** and **2d** as the most "drug-like" compounds of the whole set of new compounds.

Biological activity

AChE inhibition. The inhibitory profile of the new compounds towards AChE is presented in Table 2. The best inhibitory activities were found for **1a**, **1b**, **1c** and **2d**, presenting IC_{50} values in a low micromolar range (*ca.* 14–29 μM). Some of the most active compounds are *O*-protected HP derivatives, which may be attributed to an extra-interaction between the benzyl group and aromatic residues of the enzyme active site. In fact, the docking simulations had evidenced potential π–π stacking interaction between the HP-*O*-benzyl group and the Trp84 residue of the CAS, thus anticipating a potentially good activity for these compounds. The BTA moiety also seemed to establish aromatic interactions with the PAS residues Tyr70 and Trp279. Most of the compounds with the highest inhibitory activities belong to the series **1** (**1a**, **1b**, **1c**), which includes the benzyl group as well as one aromatic ring in the linker, to account for hydrophobic interactions within the gorge. Interestingly, among the whole set **2** of unprotected compounds, **2d** presented the second highest inhibitory activity (14.7 μM), and even much higher than its benzyl analogue, **1d** (285 μM), which presented the lowest inhibitory capacity of series **1**. In fact, this result was not predicted by the virtual screening, which suggested for **2d** the lowest degree of interactions with AChE. A further analysis of these results (Fig. 3c and S2†) indicated that the **2d** BTA group might be able to form π–π stacking with the Trp84 residue of CAS. Its 5-membered ring could also establish van der Waals interactions within the AChE gorge, and an H-bond between the HP-carbonyl and the Tyr70-OH group. The other compounds of series **2** (**2a–2c**) showed high IC_{50} values (>500 μM), thus, irrelevant inhibitory activity. Therefore, some extra mechanism, unpredicted by the preliminary docking, must subsist to rationalize a big difference between the activities of **2d** and the other unprotected BTA–HP derivatives.

Overall, the new compounds are weaker AChE inhibitors than the reference inhibitor Dnp (420-fold more potent than the best inhibitor, **1c**). This feature, however, may be counterbalanced by eventual advantages of their extra functionalities. The fact that the benzyl-protected derivatives (series **1**) gave, in general, better and reasonably good anti-AChE properties, may lead to a further approach for the design of the related carbamate-protected BTA–HP pro-drugs.

Inhibition of $A\beta_{42}$ self-induced aggregation. A number of studies with a synthetic $A\beta_{42}$ peptide have shown peptide aggregates *in vitro* with amyloid cross-β-fibrils similar to the ones found in the brains of AD patients.[39,40]

The *in vitro* Aβ aggregation can be evaluated by a method based on the fluorescence emission by using thioflavin T (ThT). ThT has been used for many years as a histologic agent for the detection of amyloid protein deposits. Its peculiar change in optical properties upon binding with the β-pleated sheet structures of amyloid fibrils, namely with

formation of an intense fluorescence band, not observed with the non-amyloidogenic conformation (unordered/α-helix) of the soluble $A\beta_{42}$ small oligomers, allows the quantification of the Aβ aggregation by monitoring the fluorescence at 446 nm (λ_{exc}) and 490 nm (λ_{em}).[41] A preliminary time scan study of the ThT signal showed that the fluorescence signal reached a plateau after 5 min and so the fluorimetric analysis was performed at this selected time.

Based on this information, the $A\beta_{42}$ sample was prepared in phosphate buffer (pH 8.0) under favorable conditions for the self-aggregation studies.[42,43] The series of newly synthesized compounds were screened to assess their inhibitory capacity of the $A\beta_{42}$ self-aggregation. $A\beta_{42}$ was incubated at 37 °C for 24 h in the presence of the ligands. Aggregation was monitored by the ThT method, as described above. Table 2 reports the values found for the fibrillogenesis inhibition by the tested compounds at 100 μM concentration.

Analysis of the results depicted in Table 2 shows that all the compounds, except **1b**, are able to inhibit $A\beta_{42}$ self-aggregation above 40% (in a concentration ratio of 1 : 5 [Aβ : I]). This set of compounds evidenced a similar order of magnitude for the percentage of aggregation inhibition, although **1c** and **2d** appeared as the most potent inhibitors. This can be explained by their conformation which allows the compounds to interact with the β-sheet of amyloid peptides without structural hindrances, therefore inhibiting their aggregation. Since all these compounds include in their structure a BTA motif, which is present in the ThT structure (Fig. 1), the mechanism involved in the inhibition of the Aβ aggregation may be rationalized by the strong affinity of BTA for the amyloid fibrils, and they may function either as β-sheet disruptor or β-sheet formation preventing agents.

Zinc-induced $A\beta_{1-42}$ aggregation

Due to the reported correlation between metal ions and the amyloid plaques, it was decided to further complement the study on activity of present compounds as Aβ anti-aggregators, but in the presence of Zn(II). The option for this metal ion circumvents the fluorescence quenching effects anticipated for paramagnetic ions Cu(II) and Fe(III). Therefore, a selection of the compounds with the best inhibitory capacity against the self-mediated Aβ aggregation (**1c** and **2d**) was evaluated for their ability to inhibit the Zn(II)-induced Aβ aggregation. The compounds were incubated for 24 h, at 37 °C, with Aβ peptide and a solution of Zn^{2+}. After incubation, a ThT solution (5 μM) was added and fluorescence measurements were carried out. As expected, the results showed that the Zn(II) could accelerate the Aβ aggregation (see Fig. S4†). Since in this case the aggregation inhibition was observed for lower concentrations of the ligand (40 μM) than for the self-mediated aggregation (100 μM), those lower concentration conditions of the ligand were used. The percentage of inhibition of zinc-mediated aggregation were 27.1 (**1c**) and 31.8 (**2d**), with 40 μM ligand concentration. Although a direct comparison between these values and the corresponding ones obtained in the absence of the zinc (68.9 for **1c**; 59.3 for **2d**, with 100 μM ligand concentration) is not possible, these results clearly indicate the existence of an order inversion on their inhibitory capacity. This result may be rationalized in terms of an interplay of two different effects enabled by these bifunctional compounds: one, due to the ligand–Aβ interactions, namely involving BTA and other groups of the ligands; another one, based on the chelating effect, because the chelating group can compete with the peptide for the metal ion and so disrupt the metal-induced aggregation. In this case, the first effect seems to be more relevant for Aβ self-aggregation, whereas in metal-mediated aggregation the chelating effect has also an important role. In fact, although the interaction of Zn^{2+} with the ligands under study is out of the scope of this paper, the Zn(II)–(3-hydroxy-4-pyridinone) systems have been previously reported.[44] This type of chelator demonstrated reasonably good affinity for the hard–soft Zn^{2+} ion (for DFP, pZn = 6.3),[44] which should be strong enough to compete with the Aβ peptide for the metal ion, but without its depletion from essential metalloproteins.

Cell viability

Efficiency of the BTA–HP based compounds in preventing $A\beta_{42}$-induced toxicity. To evaluate the potential therapeutic action of the BTA–HP based compounds, SH-SY5Y cells were treated with $A\beta_{42}$ peptides, which constitutes a good *in vitro* cellular model for studying neurodegeneration associated with AD. For that, **1b–1d**, **2a** and **2d** were tested as representative compounds. The cell proliferation assay makes use of a quantitative colorimetric method with 3-(4,5-dimethylthiazol-2-yl)-2,5-diphenyltetrazolium bromide (MTT), and accounts for the viability of the SH-SY5Y cells, with and without treatment (see the Experimental part).

Fig. 6 shows that there was a significant decrease in cell viability after a 24 h treatment with 1 μM $A\beta_{42}$ peptides (about 15% with respect to the control). At the concentrations used in these tests (2.5–7 μM of the compound), only **2d** changed the cell viability at the same end point (decreasing it about 10–15%), while all the other compounds did not make appreciable difference. Regarding the effect on the cells treated with $A\beta_{42}$ peptides, only compound **1c** improved the cell viability, restoring it to about 100% with respect to the control without $A\beta_{42}$.

An analogous assay on cell viability was also carried out in the presence of iron. Since oxidative stress is also a key feature of AD, the efficacy of compounds **1c** and **2d** was tested against such an effect mediated by iron addition. Thus, ascorbate–iron was added, assuming that it could give rise to the reactive hydroxyl radical by the iron-catalyzed Haber–Weiss reaction. However, the results of the iron effect on the cell viability were meaningless (Fig. S5†). In fact, although the addition of the iron–ascorbate pair could induce the iron reduction, the absence of any strong oxidant disabled the iron reoxidation and provoked the induced formation of the redox active species and oxidative stress in the cells.[45] On the other hand, the effect of the ligands (**1c** and **2d**) on cell viability kept the same behavior independently of the presence of iron. In fact, in spite of the demonstrated high affinity of the chelator **2d** for

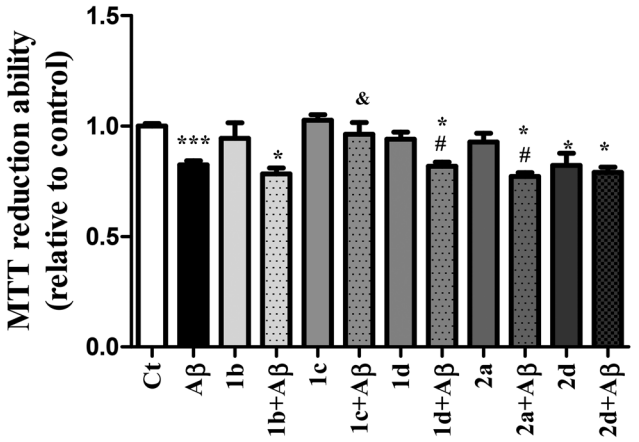

Fig. 6 Effect of BTA–HP compounds on $A\beta_{42}$ peptides toxicity. SH-SY5Y cells were treated with $A\beta_{42}$ (1 μM) peptides, for 24 h, in the absence or the presence of BTA–HP compounds. Evaluation of cell viability was performed by using the MTT reduction test. Results are expressed as the percentage of SH-SY5Y untreated cells, with the mean ± SEM derived from 3 different experiments. ***$p < 0.001$; *$p < 0.05$, significantly different when compared with SH-SY5Y untreated cells; #$p < 0.05$; significantly different when compared with $A\beta_{42}$ treated SH-SY5Y cells; &$p < 0.05$, significantly different when compared with the respective BTA–HP treated SH-SY5Y cells.

iron(III), it possesses an extremely weak affinity for iron(II), as reported for DFP.[46]

Hence, based on the data obtained in the studied cellular context, compound **1c** seems to be the most promising one to be used in further studies.

Conclusions

A set of multifunctional compounds has been developed and studied as potential drug candidates for the multifaceted Alzheimer's disease (AD). The main feature of these ligands is based on their common framework which conjugates 3-hydroxy-4-pyridinone (HP) and benzothiazole (BTA) moieties, which are well known for their high affinity for iron(III), and beta-amyloid (Aβ), respectively. Furthermore, due to the multifactorial nature of AD, the linker between those two basic molecular units was designed to provide the whole molecule with capability for the inhibition of acetylcholinesterase (AChE). Following this strategy, a set of four hybrid (3-hydroxy-4-pyridinone)–benzothiazole (HP–BTA, **2a–2d**) chelators and their HP-*O*-benzyl analogues (**1a–1d**) were prepared and evaluated for their physico-chemical and biological properties. For two representative compounds (**2a** and **2d**), the iron-complexation study confirmed their high ability to form tris-chelated complexes (FeL_3) (pFe = 19.2–19.4). The chelators displayed also significant anti-oxidant properties (in opposition to *O*-protected analogues), and the best activity was found for **2d**. Regarding the biological activity, reasonable AChE inhibitory activities (IC_{50} = 14–19 μM) were obtained for a set of compounds (**1a**, **1b**, **1c** and **2d**), which seems to be mainly rationalized in terms of interactions between lipophilic amino acid residues within the AChE active site and the phenylic and cyclic groups of the compounds, as indicated by the modeling studies. This selection of hybrid compounds evidenced also good inhibitory capacity towards $A\beta_{42}$ self-aggregation, mostly above 40%. Among the most active compounds, a chelator **2d** (59%, 100 μM) and a "pro-chelator" **1c** (68%, 100 μM), the capacity of inhibition of the $A\beta_{42}$ zinc-induced-aggregation revealed to be superior for the chelator **2d**. Overall, the anti-$A\beta_{42}$ aggregation activity of these compounds seems to result from the contribution of two main effects, namely the BTA interactions with the peptide and the metal chelation ability. Finally a cellular study on the effect of the BTA–HP based compounds in SH-SY5Y cells treated with $A\beta_{42}$, as a model of AD neurodegeneration, showed that compound **1c** presented the best efficiency in preventing $A\beta_{42}$-induced toxicity.

In brief, these preliminary findings show that this set of hybrid hydroxypyridinone–benzothiazole chelators and derivatives can merge important properties, such as iron-chelation, anti-oxidant activity, AChE inhibition and interaction with Aβ, and some of them may be further studied in view of AD drug development.

Experimental part

General methods

Analytical grade reagents were purchased from Sigma, Aldrich, Fluka, Acros, and Merck, and were used as supplied. DFP and 3-hydroxy-2-methyl-4-pyrone (maltol) were from Aldrich. An amyloid-β peptide fragment 1–42 ($A\beta_{42}$) was obtained from American Peptide Company Inc (USA). Solvents were dried according to standard methods.[47] The chemical reactions were monitored by TLC using aluminum plates coated with silica gel 60 F254 (Merck). Column flash chromatography separations were performed using silica gel Merck 230–400 mesh ASTM. The ^1H and ^{13}C NMR spectra were recorded on a Bruker ADVANCE III 300 or 400 MHz spectrometer at room temperature. Chemical shifts (δ) are reported in ppm from the internal reference TMS (tetramethylsilane), for organic solvents, and DSS (3-trimethylsilyl-propionic acid-d4 sodium salt) for D_2O. The following abbreviations are used: s = singlet, d = doublet, t = triplet, m = multiplet.

Melting points were measured with a Leica Galen III hot stage apparatus and are uncorrected. The electrospray ionization mass spectra (ESI MS) were obtained on a 500 MS LC Ion Trap (Varian Inc., Palo Alto, CA, USA) mass spectrometer equipped with an ESI ion source, operated in the positive or negative ion mode. Microanalyses were performed using a Fisons EA1108 CHNF/O instrument.

Molecular modelling

In a first approach to our drug design, a docking study was performed in order to design new potential AChE inhibitors based on previously known biologically-active molecular fragments. For that, the X-ray structures of AChE were taken from the RCSB Protein Data Bank (PDB).[31] In this case, the crystal

structure with PDB code 1EVE, corresponding to the *Torpedo californica* variant (TcAChE) complexed with donepezil (Dnp), was chosen.

Solvent and auxiliary co-crystallization molecules were removed from the original structure, and hydrogen atoms were added by means of Maestro 7.5.[48] The original ligand was extracted from the complex, and the two structures were saved separately. The ligands were drawn using Maestro, and then they were submitted to a conformational search (CS) of 1000 cycles, using a water environment model (generalized-Born/surface-area model) by means of Macromodel.[49] The algorithm used was based on the Monte Carlo method, with the molecular Merck force field (MMFFs) and a distance-dependent dielectric constant of 1.0. The lowest-energy conformation of each ligand was saved, and it was docked into the previously saved AChE structure, using the GOLD program, version 4.0.[30] The region of interest was defined in order to contain the residues within 15 Å from the position of the original ligand (Dnp). The Gold default parameters were used, and the ligands were submitted to 100 genetic algorithm runs. The ASP scoring function was used in this case, since it has previously revealed, among the ones supplied by Gold (GoldScore, ChemScore, and ASP), to give the best prediction with AChE inhibitors.[50] For each ligand, the docking solution taken into account was the conformation with the best score, according to the fitness function used, ASP.

Synthesis of the compounds

Benzyloxy-2-methyl-4-pyrone (3). To a solution of 3-hydroxy-2-methyl-4-pyrone (10 g, 79 mmol) in methanol (100 mL) with the same amount of 7 M aqueous NaOH (12 mL, 79 mmol) was added benzyl chloride (10.1 mL, 88 mmol). The mixture was left under reflux overnight.

After cooling, the mixture was filtered and evaporated to dryness. The resulting residual oil was dissolved in dichloromethane and washed with a 5% NaOH aqueous solution and water. The organic phase was dried with anhydrous sodium sulfate and the solvent was evaporated to dryness to obtain the pure product as a pale yellow oil (74% yield). ^{1}H NMR ($CDCl_3$), δ (ppm): 7.59 (1H, d, J = 5.7 Hz, 6-HPy), 7.39–7.33 (5H, 1d and 2t, Ph), 6.36 (1H, d, J = 5.4 Hz, 5-HPy), 5.16 (2H, s, CH_2), 2.09 (3H, s, CH_3). m/z (ESI MS): 217.1 $(M + H)^+$.

3-Benzyloxy-1-(3′-carboxylpropyl)-2-methyl-4-pyridinone (4a). **3** (8.27 g, 38 mmol) and amino butyric acid (3.91 g, 9.4 mmol) were dissolved in methanol (130 mL). The pH was adjusted to 13 with an aqueous solution of 10% NaOH and the mixture was left under reflux for 5 h. After cooling, the reaction mixture was evaporated. The oil obtained was dissolved in ethyl acetate and extracted with water. The aqueous phase was acidified till pH ~ 4 with a 2 M HCl solution and extracted with dichloromethane. The organic phase was dried over anhydrous sodium sulfate and evaporated till dryness. The pure product was obtained as a beige solid (48% yield). ^{1}H NMR ($CDCl_3$), δ (ppm): 7.52 (1H, d, J = 5.7 Hz, 6-HPy), 7.38–7.30 (5H, 2d and 3t, Ph), 6.58 (1H, d, J = 5.7 Hz, 5-HPy), 5.15 (2H, s, OCH_2Ph), 3.95 (2H, t, J = 10.2 Hz, CH_2N), 2.37 (2H, t, J = 9.6 Hz, CH_2-COOH), 2.16 (3H, s, CH_3), 2.01 (2H, m, $CH_2CH_2CH_2$). m/z (ESI MS): 302.1 $(M + H)^+$.

2-(4-(3-(Benzyloxy)-2-methyl-4-oxopyridin-1(4*H*)-yl)phenyl)-acetic acid (4b). **3** (2 g, 9.4 mmol) and 4-aminophenylacetic acid (1.42 g, 9.4 mmol) were dissolved in a solution of aqueous 0.1 M HCl (50 mL) in ethanol (100 mL) and the mixture was left under reflux overnight. After cooling, the reaction mixture was evaporated. The oil obtained was taken into a 5% NaOH solution and washed with dichloromethane. The aqueous phase was acidified to pH ~ 3 with 1 M HCl solution and extracted with ethyl acetate. The organic phase was dried over anhydrous sodium sulfate and evaporated till dryness. The pure product was obtained as a pale solid (23% yield). ^{1}H NMR (D_2O), δ (ppm): 7.78 (1H, d, J = 10.0 Hz, 6-HPy), 7.46–7.44 (5H, 2d and 3t, Ph), 7.42 (2H, d, J = 11.2 Hz, N-C*H*CH), 7.24 (2H, d, J = 11.2 Hz, N-CHC*H*), 6.67 (1H, d, J = 9.6 Hz, 5-HPy), 5.12 (2H, s, OCH_2-Ph), 3.62 (2H, s, CH_2-COOH), 1.81 (3H, s, CH_3). m/z (ESI MS): 350.1 $(M + H)^+$.

General procedure for the synthesis of benzothiazole derivatives 5a–5c

2-Aminothiophenol (1 mmol) and an equivalent amount of amino-carboxylic acid (*e.g.* 4-aminobenzoic acid, L-proline or 4-aminomethylbenzoic acid) were dissolved in polyphosphoric acid (PPA) and the reaction mixture was left under reflux (T ~ 220 °C) for 4 h. After cooling, the reaction mixture was dissolved in 5% NaOH aqueous solution and extracted with dichloromethane. The organic phase was then extracted with a 0.1 N HCl aqueous solution and washed with dichloromethane. The aqueous phase was basified to pH ~ 10–12 with a 5 M NaOH aqueous solution and extracted with dichloromethane. The organic phase was dried over anhydrous sodium sulfate and the solvent was evaporated.

4-(Benzo[*d*]thiazol-2-ylmethyl)aniline (5a). 2-Aminothiophenol (1.54 mL, 14.3 mmol) and 4-aminobenzoic acid (1.96 g, 14.3 mmol) give the pure hydrochloric salt as a brown solid (53% yield) after acidification with HCl-saturated methanol until pH ~ 1 and recrystallization from acetonitrile.

^{1}H-NMR (D_2O), δ (ppm): 7.98 (1H, d, J = 9 Hz, NC-CH), 7.93 (1H, d, J = 9 Hz, SC-CH), 7.56 (2H, t, J = 9 Hz, NC-CHC*H* and SC-CHC*H*), 7.50 (2H, d, J = 9 Hz, C*H*-CHNH$_2$), 7.42 (2H, d, J = 9 Hz, CHC*H*-NH$_2$), 4.57 (2H, s, CH_2). m/z (ESI MS): 241.1 $(M + H)^+$.

(4-(Benzo[*d*]thiazol-2-yl)phenyl)methanamine (5b). 4-Aminomethyl benzoic acid (1.02 g, 6 mmol) and 2-aminothiophenol (0.7 mL, 6 mmol) give the pure product as a pale greenish-blue solid (53% yield). ^{1}H-NMR ($CDCl_3$), δ (ppm): 8.08–8.05 (3H, m, NC-CH and Ph), 7.90 (1H, d, J = 7.6 Hz, SC-CH), 7.52–7.36 (4H, m, NC-CHC*H*, SC-CHC*H* and Ph), 3.96 (2H, s, CH_2). m/z (ESI MS): 241.1 $(M + H)^+$.

2-(Pyrrolidin-2-yl)benzo[*d*]thiazole (5c). 2-Aminothiophenol (1.54 mL, 14.3 mmol) and L-proline (2.92 g, 14.3 mmol) afford the pure hydrochloric salt as an orange solid (71% yield) after acidification with HCl-saturated methanol until pH ~ 1 and recrystallization from acetonitrile. ^{1}H-NMR (D_2O), δ (ppm): 8.09 (2H, d, J = 9 Hz, NC-CH and SC-CH), 7.65–7.57 (2H, 2t,

NC-CHC*H* and SC-CHC*H*), 5.28 (1H, t, *J* = 7.5 Hz, C-C*H*NH), 3.62 (2H, m, NHCH_2), 2.73 (1H, m, C-CHCH_2), 2.42 (1H, m, C-CHCH_2), 2.26 (2H, m, CHNH-CH_2). *m*/*z* (ESI MS): 205.1 $(M + H)^+$.

General procedure for the synthesis of compounds 1a–1d

5a, **5b** or **5c** (1 mmol), **4a** or **4b** (2 mmol), 1-ethyl-3-(3-dimethylaminopropyl) carbodiimide hydrochloride (EDC·HCl, 4 mmol) and a catalytic amount of 4-dimethylaminopyridine (DMAP, 5% mol) were dissolved in dichloromethane and the mixture was left stirring at room temperature overnight. The reaction mixture was washed with 5% NaOH solution, 1 M HCl solution and water. The organic phase was dried over anhydrous sodium sulfate and evaporated to dryness.

***N*-(4-(Benzo[*d*]thiazol-2-ylmethyl)phenyl)-4-(3-(benzyloxy)-2-methyl-4-oxopyridin-1(4*H*)-yl)butanamide (1a). 5a** (50 mg, 0.181 mmol) and **4a** (61 mg, 0.203 mmol) afford the pure product as a beige solid (69% yield) with recrystallization from ethyl acetate. M.p. 73–75 °C.

^{1}H NMR ($CDCl_3$), *δ* (ppm): 8.40 (1H, d, *J* = 7.5 Hz, 6-HPy), 7.98 (1H, d, *J* = 8.3 Hz, NC-CH), 7.79 (1H, d, *J* = 7.8 Hz, SC-CH), 7.55 (2H, d, *J* = 7.6 Hz, NH-C*H*), 7.45 (2H, t, *J* = 7.8 Hz, NCCH-C*H* and SCCH-C*H*), 7.36–7.32 (5H, 2d and 3t, Ph), 7.21 (2H, d, *J* = 7.6 Hz, NHCH-C*H*), 6.33 (1H, d, *J* = 7.5 Hz, 5-HPy), 5.17 (2H, s, OCH_2Ph), 4.40 (2H, s, CH_2-CN), 3.91 (2H, t, *J* = 6.9 Hz, N-CH_2CH_2), 2.35 (2H, t, *J* = 6.7 Hz, CO-CH_2), 2.14 (3H, s, CH_3), 2.02 (2H, m, CH_2CH_2CH_2). ^{13}C NMR ($CDCl_3$), *δ* (ppm): 173.2 (C═O), 171.6 (C═O), 170.3 (SC═N), 153.3 (C arom-BTA), 146.3 (C-O), 142.0 (6-CPy), 139.1 (C arom-HP), 138.2 (C arom-BTA), 137.3 (C arom-BTA), 135.7 (C arom-BTA), 132.5 (C arom-HP), 129.7 (2 × C arom-BTA), 128.9 (2 × C arom-HP), 128.5 (2 × C arom-HP), 128.3 (C arom-BTA), 126.1 (C arom-BTA), 124.9 (*C*-CH_3), 122.8 (5-Cpy), 121.7 (C arom-BTA), 120.4 (2 × C arom-HP), 116.9 (C arom-BTA), 73.20 (OCH_2-Ph), 53.15 (CH_2), 40.15 (CH_2), 32.38 (CH_2), 25.63 (CH_2), 12.56 (CH_3). *m*/*z* (ESI MS): 524.3 $(M + H)^+$. Analysis calc. for $C_{31}H_{29}N_3O_3S·H_2O$: C 68.91, H 5.76, N 7.78, S 5.93%; found: C 68.90, H 5.63, N 7.72, S 5.97%.

***N*-(4-(Benzo[*d*]thiazol-2-ylmethyl)phenyl)-2-(4-(3-(benzyloxy)-2-methyl-4-oxopyridin-1(4*H*)-yl)phenyl)acetamide (1b). 5a** (25 mg, 0.1 mmol) and **4b** (17.7 mg, 0.1 mmol) give the pure product as a pale yellow solid (73% yield) with recrystallization from ethyl acetate. M.p. 89–91 °C. ^{1}H NMR (MeOD), *δ* (ppm): 7.94 (2H, t, *J* = 9.3 Hz, NC-CHC*H* and SC-CHC*H*), 7.71 (1H, d, *J* = 7.5 Hz, 6-HPy), 7.59 (4H, m, Ph), 7.52 (2H, m, Ph), 7.47–7.31 (9H, m, NHC-C*H*, NC-C*H*CH, NC-CH, Ph), 6.59 (1H, d, *J* = 7.5 Hz, 5-HPy), 5.17 (2H, s, OCH_2Ph), 4.45 (2H, s, CH_2C═N), 3.81 (2H, s, CH_2CONH), 1.92 (3H, s, CH_3). ^{13}C NMR (MeOD), *δ* (ppm): 175.2 (C═O), 173.9 (C═O), 171.3 (SC═N), 146.6 (C-O), 145.4 (*C*-CH_3), 141.8 (C arom-HP), 141.3 (6-CPy), 139.1 (C arom-BTA), 138.5 (C arom-BTA), 134.5 (C arom-BTA), 132.0 (2 × C arom-BTA), 130.7 (2 × C arom-HP), 130.3 (2 × C arom-HP), 129.4 (2 × C arom-HP), 129.3 (C arom-HP), 127.9 (2 × C arom-HP), 127.4 (C arom-BTA), 126.3 (C arom-HP), 123.2 (C arom-BTA), 122.9 (C arom-BTA), 121.6 (2 × C arom-BTA), 117.0 (5-Cpy), 74.64 (OC-Ph), 43.95 (CH_2), 40.31 (CH_2), 14.89 (CH_3). *m*/*z* (ESI MS): 594.0 $(M + Na)^+$. Analysis calc. for $C_{35}H_{29}N_3O_3S·1.5H_2O$: C 70.29, H 5.38, N 7.03, S 5.36%; found: C 70.34, H 5.55, N 6.67, S 5.38%.

***N*-(4-(Benzo[*d*]thiazol-2-yl)benzyl)-2-(4-(3-(benzyloxy)-2-methyl-4-oxopyridin-1(4*H*)-yl)phenyl)acetamide (1c). 4b** (51 mg, 0.146 mmol) and **5b** (33 mg, 0.138 mmol) afford the pure product as a pale green solid (70% yield) with recrystallization from ethyl ether. M.p. 93–95 °C.

^{1}H NMR (MeOD), *δ* (ppm): 8.03 (4H, m, Ph), 7.67 (1H, d, *J* = 7.4 Hz, 6-HPy), 7.53 (3H, m, SC-CH, NC-CH and NHC-C*H*), 7.45 (5H, m, Ph) 7.35 (3H, m, NC-CHC*H*, SC-CHC*H* and Ph), 7.29 (2H, m, Ph), 6.55 (1H, d, *J* = 7.4 Hz, 5-HPy), 5.15 (2H, s, OCH_2Ph), 4.49 (2H, s, CH_2-NH), 3.70 (2H, s, CH_2CONH), 1.88 (3H, s, CH_3). ^{13}C NMR (MeOD), *δ* (ppm): 210.0 (C═O), 201.0 (C═O), 194.4 (SC═N), 191.4 (C-O), 175.1 (*C*-CH_3), 173.2 (C arom-HP), 143.7 (C arom-BTA), 141.8 (C arom-BTA), 141.6 (6-CPy), 139.3 (C arom-BTA), 138.4 (2 × C arom-BTA), 131.9 (2 × C arom-HP), 130.3 (2 × C arom-HP), 129.4 (2 × C arom-HP), 129.3 (C arom-HP), 128.7 (2 × C arom-HP), 127.9 (C arom-BTA), 127.8 (C arom-HP), 126.7 (C arom-BTA), 123.8 (C arom-BTA), 123.0 (2 × C arom-BTA), 116.9 (5-Cpy), 74.70 (OC-Ph), 30.67 (CH_2), 24.23 (CH_2), 14.92 (CH_3). *m*/*z* (ESI MS): 572.1 $(M + H)^+$. Analysis calc. for $C_{35}H_{29}N_3O_3S·0.3Et_2O$: C 70.08, H 5.22, N 6.76, S 5.15%; found: C 70.15, H 4.85, N 6.45, S 4.88%.

1-(4-(2-(Benzo[*d*]thiazol-2-yl)pyrrolidin-1-yl)-4-oxobutyl)-3-(benzyloxy)-2-methylpyridin-4(1*H*)-one (1d). 4a (1 g, 3.32 mmol) and **5c** (80 mg, 3.32 mmol) afford the pure product as a hygroscopic orange solid (80% yield) with recrystallization from ethyl acetate. ^{1}H NMR (MeOD), *δ* (ppm): 7.93 (2H, m, NC-CH and SC-CH), 7.69 (1H, d, *J* = 7.4 Hz, 6-HPy), 7.54–7.31 (7H, m, NC-CHC*H*, SC-CHC*H* and Ph), 6.48 (1H, d, *J* = 7.4 Hz, 5-HPy), 5.47 (1H, m, N-CH-C═N), 5.07 (2H, s, OCH_2Ph), 4.02 (2H, t, *J* = 7.7 Hz, N-CH_2CH_2CH_2), 3.68 (2H, m, N-CH_2CH_2), 2.50 (2H, t, *J* = 7.7 Hz, CH_2-CO), 2.41 (1H, m, NCH-CH_2), 2.23 (1H, m, NCH-CH_2), 2.18 (3H, s, CH_3), 1.96 (2H, m, N-CH_2CH_2). ^{13}C NMR (MeOD), *δ* (ppm): 176.3 (C═O), 174.8 (C═O), 173.1 (SC═N), 154.2 (C-N), 145.2 (C-O), 141.1 (6-CPy), 138.5 (C arom-HP), 135.8 (C-S), 130.3 (2 × C arom-HP), 129.4 (2 × C arom-HP), 129.3 (C arom-HP), 127.4 (C arom-BTA), 126.4 (C arom-BTA), 123.4 (C arom-BTA), 123.3 (C arom-BTA), 123.0 (*C*-CH_3), 117.4 (5-Cpy), 74.48 (OC-Ph), 60.60 (CH-N), 54.50 (CH_2), 47.89 (CH_2), 33.48 (CH_2), 31.34 (CH_2), 26.36 (CH_2), 25.25 (CH_2), 12.80 (CH_3). *m*/*z* (ESI MS): 488.3 $(M + H)^+$. Analysis calc. for $C_{28}H_{29}N_3O_3S·0.1HCl·0.8H_2O$: C 66.66, H 6.13, N 8.33, S 6.36%; found: C 66.68, H 6.13, N 8.48, S 5.96%.

General procedure for the synthesis of 6a and 6b

In a hydrogenation flask, **4a** or **4b** (1 mmol) was dissolved in methanol and 10% Pd/C was added (10% w/w). The reaction suspension was left for 2 h under H_2 atmosphere at 2 bar pressure. The reaction mixture was filtered and the solvent was evaporated to dryness, affording the pure product.

4-(3-Hydroxy-2-methyl-4-oxopyridin-1(4*H*)-yl)butanoic acid (6a). 4a (200 mg, 0.664 mmol) afforded the pure product as a pale brown solid (95% yield). ^{1}H NMR (MeOD), *δ* (ppm): 7.62 (1H, d, *J* = 7.2 Hz, 6-HPy), 6.41 (1H, d, *J* = 7.2 Hz, 5-HPy), 4.10 (2H, t, *J* = 7.65 Hz, CH_2N), 2.47 (3H, s, CH_3), 2.40 (2H, t, *J* =

6.9 Hz, CH_2-COOH), 2.02 (2H, m, $CH_2CH_2CH_2$). *m*/*z* (ESI MS): 212.1 $(M + H)^+$.

2-(4-(3-Hydroxy-2-methyl-4-oxopyridin-1(4*H*)-yl)phenyl)acetic acid (6b). **4b** (200 mg, 0.573 mmol) afforded the pure product as a light brown solid (93% yield). ^{1}H NMR (MeOD), δ (ppm): 7.59 (1H, d, J = 7.2 Hz, 6-HPy), 7.53 (2H, d, J = 8.1 Hz, Ph), 7.35 (2H, d, J = 8.1 Hz, Ph), 6.48 (1H, d, J = 7.2 Hz, 5-HPy), 3.73 (2H, s, CH_2), 2.13 (3H, s, CH_3). *m*/*z* (ESI MS): 259.2 $(M + H)^+$.

General procedure for the synthesis of compounds 2a–2d

A solution of **6a** or **6b** (1 mmol) in dry dichloromethane under a nitrogen atmosphere was cooled over an ice–salt–water bath. Ethylchloroformate (ECF, 2.1 mmol) and *N*-methylmorpholine (NMM, 4 mmol) were added and the reaction mixture was left reacting for 40 min. Then, **5a**, **5b** or **5c** (1.1 mmol) was added and the reaction mixture was left at room temperature for 3 h. The reaction mixture was filtered and the solvent was evaporated. The oil obtained was dissolved in ethyl acetate and washed with water and a solution of 0.05 M HCl. The organic phase was dried under anhydrous sodium sulfate and evaporated to dryness.

The solid was taken in an aqueous solution of 2% $NaHCO_3$–EtOH (1 : 1) and left at ~65 °C for 4 h. The reaction mixture was evaporated and the oil obtained was dissolved in ethyl acetate (for all compounds, except for **2d** that is dissolved in dichloromethane) and washed with water. The organic phase was dried under anhydrous sodium sulfate and evaporated till dryness. The solid obtained was recrystallized with diethyl ether to afford the pure product.

***N*-(4-(Benzo[*d*]thiazol-2-ylmethyl)phenyl)-4-(3-hydroxy-2-methyl-4-oxopyridin-1(4*H*)-yl)butanamide (2a).** From **6a** (80 mg, 0.379 mmol) and **5a** (81 mg, 0.293 mmol), the general method afforded the pure product as a beige solid (29% yield). M.p. 91–93 °C. ^{1}H NMR (MeOD), δ (ppm): 7.94 (2H, t, J = 9.2 Hz, NCC*H*-CH and SCC*H*-CH), 7.71 (1H, d, J = 6.8 Hz, 6-HPy), 7.57–7.49 (3H, 2d and 1t, J = 8.3 Hz, NC-CH and Ph), 7.42–7.34 (3H, 1t and 2d, SC-CH and Ph), 6.49 (1H, d, J = 6.8 Hz, 5-HPy), 4.43 (2H, s, CH_2-CN), 4.19 (2H, t, J = 7.4 Hz N-CH_2CH$_2$), 2.49 (2H, m, CO-CH_2), 2.16 (2H, t, J = 7.4 Hz, $CH_2CH_2CH_2$), 2.03 (3H, s, CH_3). ^{13}C NMR (DMSO), δ (ppm): 171.4 (C═O), 170.1 (C═O), 145.2 (SC═N), 138.1 (C-O), 137.6 (6-CPy), 135.0 (*C*-CH_3), 135.8 (C-S and C-N), 129.5 (2 × C arom), 126.1 (C arom), 124.9 (C arom), 122.3 (C arom), 122.1 (C arom), 119.5 (2 × C arom), 110.6 (5-Cpy), 56.09 (CH_2), 52.53 (CH_2), 32.45 (CH_2), 25.86 (CH_2), 11.39 (CH_3). *m*/*z* (ESI MS): 434.1 $(M + H)^+$. Analysis calc. for $C_{24}H_{23}N_3O_3S{\cdot}H_2O$: C 63.98, H 5.57, N 9.33, S 7.12%; found: C 64.02, H 5.56, N 9.15, S 6.91%.

***N*-(4-(Benzo[*d*]thiazol-2-ylmethyl)phenyl)-2-(4-(3-hydroxy-2-methyl-4-oxopyridin-1(4*H*)-yl)phenyl)acetamide (2b).** From **6b** (60 mg, 0.232 mmol) and **5a** (70 mg, 0.255 mmol), the general method afforded the pure product as a beige solid (20% yield). M.p. 75–77 °C. ^{1}H NMR ($CDCl_3$), δ (ppm): 7.97 (1H, d, J = 6.3 Hz, 6-HPy), 7.78 (1H, d, J = 8.0 Hz, NC-CH), 7.67 (1H, d, J = 8.0 Hz, SC-CH), 7.51 (2H, d, J = 7.2 Hz, NHC-CH), 7.45 (2H, t, J = 8.0 Hz, NC-CHCH and SC-CHCH), 7.34 (2H, d, J = 7.2 Hz, NHC-CHCH), 7.23 (1H, d, J = 5.7 Hz, NC-CHCH), 7.14 (2H, d, J = 5.7 Hz, NC-CH), 6.45 (1H, d, J = 7.2 Hz, 5-HPy), 4.40 (2H, s, CH_2CONH), 3.80 (2H, s, CH_2CN), 2.11 (3H, s, CH_3). ^{13}C NMR (MeOD), δ (ppm): 171.7 (C═O), 171.5 (C═O), 146.9 (SC═N), 142.1 (C-O), 139.5 (6-CPy), 139.2 (C-N), 139.0 (C-S), 137.9 (C arom-BTA), 136.7 (C arom-BTA), 134.5 (*C*-CH_3), 133.1 (2 × C arom-HP), 132.1 (2 × C arom-BTA), 130.8 (2 × C arom-HP), 128.1 (2 × C arom-BTA), 127.5 (C arom-BTA), 126.4 (C arom-BTA), 123.2 (C arom-BTA), 122.9 (C arom-BTA), 121.7 (2 × C arom-HP), 112.7 (5-Cpy), 44.05 (CH_2), 40.39 (CH_2), 13.71 (CH_3). *m*/*z* (ESI MS): 482.3 $(M + H)^+$. Analysis calc. for $C_{28}H_{23}N_3O_3S{\cdot}0.2HCl$: C 65.63, H 4.67, N 8.13, S 6.21%; found: C 65.68, H 4.52, N 7.46, S 6.68%.

***N*-(4-(Benzo[*d*]thiazol-2-yl)benzyl)-2-(4-(3-hydroxy-2-methyl-4-oxopyridin-1(4*H*)-yl)phenyl)acetamide (2c).** From **6b** (103 mg, 0.397 mmol) and **5b** (105 mg, 0.437 mmol) the general method afforded the pure product as a light yellow solid (28% yield). M.p. 96–98 °C.

^{1}H NMR ($CDCl_3$), δ (ppm): 8.06 (1H, d, J = 7.5 Hz, 6-HPy), 7.92 (1H, d, J = 7.8 Hz, NC-CH), 7.67 (1H, d, J = 7.8 Hz, SC-CH), 7.43 (2H, d, J = 7.2 Hz, NHC-CH), 7.40 (2H, t, J = 9.3 Hz, NC-CHCH and SC-CHCH), 7.37 (2H, d, J = 7.2 Hz, NHC-CHCH), 7.34 (1H, d, J = 7.2 Hz, NC-CHCH), 7.16 (2H, d, J = 9.0 Hz, NC-CH), 6.56 (1H, d, J = 7.5 Hz, 5-HPy), 4.54 (2H, d, J = 5.7 Hz, CH_2-NH), 3.70 (2H, s, CH_2CONH), 1.89 (3H, s, CH_3). ^{13}C NMR (MeOD), δ (ppm): 184.7 (SC═N), 143.7 (C-O), 139.4 (*C*-CH_3), 134.6 (6-CPy), 131.8 (2 × C arom-BTA), 129.4 (C arom-BTA), 128.7 (2 × C arom-HP), 128.0 (2 × C arom-BTA), 127.8 (C arom-BTA), 126.7 (C arom-BTA), 123.8 (C arom-HP), 122.9 (2 × C arom-HP), 112.6 (5-Cpy), 44.03 (CH_2), 43.30 (CH_2), 13.81 (CH_3). *m*/*z* (ESI MS): 482.0 $(M + H)^+$. Analysis calc. for $C_{28}H_{23}N_3O_3S{\cdot}1.4EtOH$: C 64.77, H 5.27, N 7.72, S 5.89%; found: C 64.85, H 4.99, N 7.26, S 5.74%.

1-(4-(2-(Benzo[*d*]thiazol-2-yl)pyrrolidin-1-yl)-4-oxobutyl)-3-hydroxy-2-methylpyridin-4(1*H*)-one (2d). From **6a** (234 mg, 1.11 mmol) and **5c** (293 mg, 1.22 mmol), the general method afforded the pure product as a beige solid (15% yield). M.p. 83–85 °C.

^{1}H NMR (MeOD), δ (ppm): 7.94 (2H, t, J = 9.4 Hz, NC-CH and SC-CH), 7.63 (1H, d, J = 7.2 Hz, 6-HPy), 7.52–7.42 (2H, m, NCCH-C*H* and SCCH-C*H*), 6.41 (1H, d, J = 7.2 Hz, 5-HPy), 5.49 (1H, m, N-CH-C═N), 4.11 (2H, t, J = 7.6 Hz, N-CH_2CH$_2$CH$_2$), 3.84 (2H, m, N-CH_2CH$_2$), 3.67 (2H, m), 2.56 (2H, t, J = 7.6 Hz, CO-CH_2), 2.20 (3H, s, CH_3), 2.13 (2H, m, NCH-CH_2), 1.96 (2H, m, N-CH_2CH_2). ^{13}C NMR (MeOD), δ (ppm): 176.3 (C═O), 173.2 (C═O), 170.6 (SC═N), 154.1 (C-N), 147.3 (C-OH), 138.8 (6-CPy), 135.8 (C-S), 132.9 (C arom-BTA), 127.4 (C arom-BTA), 126.4 (C arom-BTA), 123.3 (C arom-BTA), 123.0 (*C*-CH_3), 112.7 (5-Cpy), 60.58 (CH-N), 54.39 (CH_2), 47.89 (CH_2), 33.49 (CH_2), 31.42 (CH_2), 26.54 (CH_2), 25.22 (CH_2), 11.88 (CH_3). *m*/*z* (ESI MS): 398.1 $(M + H)^+$. Analysis calc. for $C_{21}H_{23}N_3O_3S{\cdot}0.2H_2O{\cdot}0.2EtOH$: C 62.13, H 5.94, N 10.27, S 7.84%; found: C 62.13, H 5.94, N 10.37, S 7.72%.

Spectroscopic studies

Solutions. The aqueous $FeCl_3$ stock solution (1.77×10^{-2} M), prepared in acid medium, was obtained from Merck and standardized by atomic absorption. Its exact HCl content was

determined by titration with 0.1 M HCl (Titrisol) for values of pH ≥ 2. The titrant solution (0.1 M KOH) was prepared from a carbonate-free commercial concentrate (Titrisol), in a 50% w/w DMSO–H_2O medium, standardized by potentiometric titration with potassium hydrogen phthalate and discarded when the percentage of carbonate (Gran's method)[51] was about 0.5% of the total amount of base. An HCl solution (0.099 M) in 50% DMSO–H_2O was used for the electrode calibration and for the batch titrations at pH ≤ 2.

Measurements. Spectrophotometric titrations (250–370 nm) of **2a** (4.0×10^{-5} M) and **2d** (8.0×10^{-5} M) were performed in 50% w/w DMSO–H_2O solution at ionic strength (I) 0.1 M KCl and the working temperature was maintained at 25.0 ± 0.1 °C. The iron complexation studies were also done by spectrophotometric titration (300–700 nm) at a 1 : 3 Fe–L stoichiometry (C_L = 1–1.5 × 10^{-4} M, 10% excess of ligand). Solutions of complexes with pH ≥ 2 were prepared with a total volume solution of 20 mL and for pH ≤ 2 (1.2–2), using a batch titration (5 points), in which the amounts of acid and KCl to be added were calculated for the total volume of the solution used (4 mL). All titrations were done in duplicate or triplicate and for comparison purposes the protonation and global iron stability constants in 50% w/w DMSO–H_2O were also calculated for DFP ($C_L = 3 \times 10^{-4}$ M) from spectrophotometric data. Under the experimental conditions used, the value determined for pK_w was 14.11.

Calculation of equilibrium constants. The stepwise protonation constants of the compounds, $K_i = [H_iL]/[H_{i-1}L][H]$, and the overall iron-complex stability constants, $\beta_{Fe_mH_bL_l} = [Fe_mH_hL_l]/[Fe]^m[H]^h[L]^l$, were calculated by fitting analysis of the spectroscopic data (PSEQUAD program[32]) in the presence and in the absence of Fe^{3+}. The Fe^{3+} hydrolytic species under the defined experimental conditions (I = 0.1 M KCl, 50% w/w DMSO–H_2O, T = 25.0 ± 0.1 °C), herein determined by potentiometry with the use of the HYPERQUAD program,[52] were included in the equilibrium model (log $\beta_{FeH_{-1}}$ = −4.07, log $\beta_{FeH_{-3}}$ = −11.42) and the species distribution curves were plotted with the HYSS program.[52]

Acetylcholinesterase inhibition

The determination of the AChE inhibitory capacity of the synthesized compounds was performed by an adaptation of a method previously described.[50] The buffer used for the enzymatic tests was 2-[4-(2-hydroxyethyl)piperazin-1-yl]ethanesulfonic acid (HEPES) 50 mM at pH 8. The Ellman reagent, 5,5′-dithiobis-(2-nitrobenzoic acid) (DTNB, 3 mM), was dissolved in a solution of buffer previously prepared (HEPES 50 mM, pH 8, NaCl 50 mM, $MgCl_2$ 20 mM). The substrate of the enzyme used in the tests was acetylthiocholine iodide (AChI, 15 mM of stock solution). The AChE (0.05 U mL^{-1}) extracted from *Electrophorus electricus* was purchased from Sigma-Aldrich and diluted in the buffer solution (HEPES 50 mM, pH 8). A stock solution of the inhibitor was prepared in methanol.

374 μL of HEPES (50 mM, pH 8), 476 μL of DTNB, 10, 20, 30, 40 or 50 μL of a stock solution of the inhibitor, 25 μL of AChE solution and the amount of methanol necessary to have 0.925 mL of the sample were mixed in a cell and left to incubate for 15 min. Subsequently, 75 μL of AChI were added. The initial rate of the enzymatic reaction was followed by reading the solution absorbance at 405 nm during the first 5 min of the reaction. For that, a Perkin-Elmer Lambda 35 UV-Vis spectrophotometer was used. Samples were prepared diluting the inhibitors in methanol, in a range of different concentrations. A control reaction was carried out using no inhibitor, and it was considered 100% activity. The percentage of inhibition (%I) was calculated by eqn (1), in which

$$\%I = 100 - \left(\frac{v_I}{v_0} \times 100\right) \quad (1)$$

v_I is the initial rate in the presence of the inhibitor and v_0 is the initial rate of the control reaction.

The inhibition curves were obtained by plotting the relation percentage of enzymatic inhibition *vs.* inhibitor concentration and a calibration curve was drawn from which the linear regression parameters were obtained.

Anti-oxidant activity

The anti-oxidant activity was measured by the 2,2-diphenyl-1-picrylhydrazyl radical (DPPH) method, as described by Tepe *et al.*[53] To a 2.5 mL solution of DPPH, four samples of compound solution with different volumes were added. The volume required for the 3.5 mL total volume was attained with methanol. The mixtures were incubated for 30 min at room temperature. The absorbance was measured at 517 nm against the corresponding blank. The control solution corresponds to the sample with only DPPH and methanol. The anti-oxidant activity was calculated using eqn (2), in which AA

$$\%AA = \frac{A_{sample} - A_{DPPH}}{A_{DPPH}} \times 100 \quad (2)$$

is the anti-oxidant activity, A_{sample} is the absorbance of the sample compound against the blank and A_{DPPH} is the absorbance of the DPPH solution (control solution) against the blank. The compound concentrations provided 50% of anti-oxidant activity (EC_{50}) by plotting the anti-oxidant activity against the compound concentration.

Inhibition of self-mediated Aβ (1–42) aggregation

An amyloid β-peptide (1–42) ($A\beta_{1-42}$) was purchased from Biopeptide Co. Inc. as a lyophilized powder and stored at −20 °C. Following a reported protocol,[42] samples were treated with 1,1,1,1,1,1-hexafluoropropan-2-ol (HFIP) to avoid self-aggregation and reserved. HFIP pre-treated $A\beta_{42}$ samples were resolubilized with a CH_3CN–Na_2CO_3 (300 μM)–NaOH (250 μM) (48.3 : 48.3 : 4.3, v/v/v) solvent mixture in order to have a stable stock solution. This $A\beta_{42}$ alkaline solution (500 μM) was diluted in phosphate buffer (0.215 M, pH 8.0) to obtain a 20 μM solution. Compounds under study were firstly dissolved in methanol (1 mg mL^{-1}), due to their hydrophobic nature, and then further diluted in phosphate buffer to the final concentration of 100 μM.

To study the $A\beta_{42}$ aggregation inhibition, a known spectrofluorimetric method, based on the fluorescence emission of thioflavin T (ThT), was followed.[42,43] Firstly, $A\beta_{42}$ (10 μL) samples and the tested compounds (10 μL) were diluted with the phosphate buffer to a 20 μM final concentration of (Aβ) and 100 μM compound concentration, and then they were incubated for 24 h at 37 °C, without stirring. As for the control, a sample of the peptide was incubated under identical conditions but without the inhibitor. After incubation, the samples were added to a black, flat and clear bottom 96-well plate (BD Falcon) with 180 μL of 1.5 μM ThT (Sigma CAS 2390-54-7) in 50 mM glycine–NaOH (pH 8.5). Blank samples were prepared for each concentration in a similar way, devoid of peptides. After 5 min incubation with the dye, the fluorescence of ThT was measured using a Spectramax Gemini EM (Molecular Devices) at the wavelength 490 nm (emission) with excitation at 446 nm. The percentage inhibition of the self-induced aggregation due to the presence of the test compound was calculated using eqn (3), where IF_i and IF_0 correspond to the fluorescence intensities in the presence and absence

$$\%I = 100 - \left(\frac{IF_i}{IF_0} \times 100\right) \quad (3)$$

of the test compound, respectively, minus the fluorescence intensities due to the respective blanks. The reported values were obtained as the mean ± SEM from two different experiments, each one made in duplicate.

Inhibition of metal-induced $A\beta_{1-42}$ aggregation

The preparation of the $A\beta_{1-42}$ solutions was similar to that described above for the self-induced method. To study the effects of **1c** and **2d** on metal-induced $A\beta_{1-42}$ aggregation a reported protocol was followed.[22] Solutions of Zn^{2+} were prepared from dilution of a 0.016 M $ZnCl_2$ standard solution to final concentration of 200 μM, using phosphate buffer (0.2 M at pH 8.0). Solutions of the compounds **1c** and **2d** were prepared in methanol for storage and diluted with phosphate buffer before use.

$A\beta_{1-42}$ (20 μM) was incubated with Zn^{2+} (20 μM) in phosphate buffer with or without the ligand (40 μM). The incubation was performed at 37 ° C for 24 h. After the incubation, the samples were diluted with 170 μL of glycine–NaOH buffer (50 mM, pH 8.5) containing thioflavin-T (5 μM). Fluorescence was measured at 450 nm (λ_{exc}) and 485 (λ_{em}) using a Spectramax Gemini EM (Molecular Devices).

Cell line and treatment

Human neuroblastoma SH-SY5Y cell lines (ATCCCRL-2266) were grown in 75 cm^2 tissue flasks in DMEM and Ham's F12 medium with 10% supplemental non-dialyzed fetal bovine serum and 100 IU mL^{-1} penicillin and 50 μg mL^{-1} streptomycin. Cells were maintained at 37 °C in a humidified incubator under an atmosphere of 95% air and 5% CO_2.

For the MTT assay, the cells were plated in 24-well plates at a density of 0.1×10^6 cells per well. 24 h after seeding the cells the medium was refreshed, and 1 μM of $A\beta_{42}$ peptide was added from a 1 mM stock solution of 276.9 μM, prepared in sterile water, for 24 h. Low-molecular weight oligomers of $A\beta_{42}$ were preferentially detected in the fresh preparations used.[54]

The tested compounds (**1b–1d**, **2a** and **2d**) were dissolved in DMSO at a concentration of 10 mM and aliquots were stored at −20 °C. These compounds were added to the medium at 5 μM (**1c**), 2.5 μM (**2a**, **2d**), or 7 μM (**1b**, **1d**) final concentrations. Before the addition of $A\beta_{42}$, the cells were pre-incubated for 2 h with the BTA–HP compounds.

In addition, the pair ascorbate (0.8 mM)–iron (2.5 μM) was added to the cells, alone or with $A\beta_{42}$ peptide, in the presence or absence of compounds **1c** and **2d**.

The final concentration of DMSO in culture media did not exceed 0.05% (v/v) and no alterations in cells were observed. For all conditions tested, control experiments were performed in which the compounds tested, $A\beta_{42}$ or ascorbate/iron were not added.

MTT cell proliferation assay

Cell reduction ability as a surrogate of cell viability was measured by using a quantitative colorimetric assay with 3-(4,5-dimethylthiazol-2-yl)-2,5-diphenyltetrazolium bromide (MTT) according to the Mosmann method.[55] In viable cells, cellular dehydrogenases metabolize MTT into a formazan that absorbs light at 570 nm. Following the cell treatment protocol the medium was aspirated and 0.5 mL MTT (0.5 mg mL^{-1}) was added to each well. The plate was then incubated at 37 °C for 2 h. At the end of the incubation period the formazan precipitates were solubilized with 0.5 mL of acidic isopropanol (0.04 M HCl–isopropanol). The absorbance was measured at 570 nm using a Spectramax Plus 384 spectrophotometer (Molecular Devices). Cell reduction ability was expressed relatively to control values obtained for untreated cells.

Abbreviations

AD	Alzheimer's disease
Aβ	Beta-amyloid
ACh	Acetylcholine
AChE	Acetylcholinesterase
AChI	Acetylcholine iodide
ROS	Reactive oxygen species
3,4-HP	3-Hydroxy-4-pyridinones
HP	Hydroxypyridinone
BTA	Benzothiazole
DFP	Deferiprone
CAS	Catalytic active site
PAS	Peripheral active site
Dnp	Donepezil
DPPH	2,2-Diphenyl-1-picrylhydrazyl radical
$A\beta_{42}$	Amyloid-β peptide fragment 1–42
MTT	(3-(4,5-Dimethylthiazol-2-yl)-2,5-diphenyltetrazolium bromide)

Acknowledgements

The authors thank the Portuguese NMR Network (IST-UTL Center) for providing access to the NMR facilities as well as the Portuguese *Fundação para a Ciência e Tecnologia* (FCT) for financial support with the project PEst-OE/QUI/UI0100/2011 and the post-Doc grant SFRH/BPD/29874/2006 (S.M. Marques). We also wish to thank Prof. Adriano Martinelli, from the University of Pisa for allowing us to use QikProp software, in order to obtain the estimation of the pharmacokinetic properties of the compounds.

References

1 C. L. Masters, R. Cappai, K. J. Barnham and V. L. Villemagne, *J. Neurochem.*, 2006, **97**, 1700.
2 M. Citron, *Nat. Rev. Drug Discovery*, 2010, **9**, 387.
3 R. Jakob-Roetne and H. Jacobsen, *Angew. Chem., Int. Ed.*, 2009, **48**, 3030.
4 H. W. Querfurth and F. M. La Ferla, *N. Engl. J. Med.*, 2010, **362**, 329.
5 A. Abbott, *Nature*, 2008, **456**, 161.
6 M. Stefani and C. M. Dobson, *J. Mol. Med.*, 2003, **81**, 678.
7 K. J. Barnham, C. L. Masters and A. I. Bush, *Nat. Rev. Drug Discovery*, 2004, **3**, 205.
8 A. I. Bush, *Curr. Opin. Chem. Biol.*, 2000, **4**, 184.
9 F. Zhou and G. Millhauser, *Coord. Chem. Rev.*, 2012, **256**, 2285.
10 H. Kozlowski, *Coord. Chem. Rev.*, 2012, **256**, 2129.
11 A. I. Bush and R. E. Tanzi, *Neurotherapeutics*, 2008, **5**, 421.
12 A. I. Bush, *Trends Neurosci.*, 2003, **26**, 207.
13 A. I. Mot, A. G. Wedd, L. Sinclair, D. R. Brown, S. J. Collins and M. W. Brazier, *Expert Rev. Neurother.*, 2011, **11**, 1717.
14 C. Rodríguez-Rodríguez, M. Telpoukhovskaia and C. Orvig, *Coord. Chem. Rev.*, 2012, **256**, 2308.
15 J. Kao and G. Grossberg, *Cholinesterase inhibitors*, in *Alzheimer's Disease*, ed. I.-F. Lau and M. A. Brodney, Springer-Verlag, Berlin, 2008, pp. 26–51.
16 U. Cornelli, *Neurodegener. Dis.*, 2010, **7**, 193.
17 Y. Biran, C. L. Masters, K. J. Barnham, A. I. Bush and P. A. Adlard, *J. Cell. Mol. Med.*, 2009, **13**, 61.
18 A. Cavali, M. L. Bolognesi, A. Minarini, M. Rosini, V. Tumiatti, M. Recanatini and C. Melchiorre, *J. Med. Chem.*, 2008, **51**, 347.
19 H. Zheng, M. B. H. Youdim and M. Fridkin, *J. Med. Chem.*, 2009, **52**, 4095.
20 M. A. Santos, S. M. Marques and S. Chaves, *Coord. Chem. Rev.*, 2012, **256**, 240.
21 K. Serdons, K. Van Laere, P. Janssen, H. F. Kung, G. Bormans and A. Verbruggen, *J. Med. Chem.*, 2009, **52**, 7090.
22 L. Huang, C. Lu, Y. Sun, F. Mao, Z. Luo, T. Su, H. Jiang, W. Shan and X. Li, *J. Med. Chem.*, 2012, **55**, 8483.
23 A. K. Sharma, S. T. Pavlova, J. Kim, D. Finkelstein, N. J. Hawco, N. P. Rath, J. Kim and L. M. Mirica, *J. Am. Chem. Soc.*, 2012, **134**, 6625.
24 A. Dedeoglu, K. Cormier, S. Payton, K. A. Tseitlin, J. N. Kremsky, L. Lai, X. Li, R. D. Moir, R. E. Tanzi, A. I. Bush, N. W. Kowall, J. T. Rogers and X. Huang, *Exp. Gerontol.*, 2004, **39**, 1641.
25 L. E. Scott, M. Telpoukhovskaia, C. Rodríguez-Rodríguez, M. Merkel, M. L. Bowen, B. D. G. Page, D. E. Green, T. Storr, F. Thomas, D. D. Allen, P. R. Lockman, B. O. Patrick, M. J. Adam and C. Orvig, *Chem. Sci.*, 2011, **2**, 642.
26 S. Gupta, A. Fallarero, P. Järvinen, D. Karlsson, M. S. Johnson, P. M. Vuorela and C. G. Mohan, *Bioorg. Med. Chem. Lett.*, 2011, **21**, 151105.
27 W. Luo, Y. P. Li, Y. He, S. L. Huang, J. H. Tan, T. M. Ou, D. Li, L. Q. Gu and Z. S. Huang, *Bioorg. Med. Chem.*, 2011, **19**, 763.
28 L. Huang, Z. Luo, F. He, J. Lu and X. Li, *Bioorg. Med. Chem.*, 2010, **18**, 4475.
29 M. L. Bolognesi, A. Cavalli, L. Valgimigli, M. Bartolini, M. Rosini, V. Andrisano, M. Recanatini and C. Melchiorre, *J. Med. Chem.*, 2007, **50**, 6446.
30 G. Jones, P. Willett, R. C. Glen, A. R. Leach and R. Taylor, *J. Mol. Biol.*, 1997, **267**, 727.
31 H. M. Berman, J. Westbrook, Z. Feng, G. Gilliland, T. N. Bhat, H. Weissig, I. N. Shindyalov and P. E. Bourne, *Nucleic Acids Res.*, 2000, **28**, 235; http://www.pdb.org/pdb/home/home.do (accessed on February–May 2011).
32 L. Zékány, I. Nagypál and G. Peintler, *PSEQUAD 501*, 2001.
33 E. T. Clarke and A. E. Martell, *Inorg. Chim. Acta*, 1992, **196**, 185.
34 M. Born, *Z. Phys.*, 1920, **1**, 45.
35 E. T. Clarke and A. E. Martell, *Inorg. Chim. Acta*, 1992, **191**, 57–63.
36 S. Chaves, S. Canário, M. Carrasco, L. Mira and M. A. Santos, *J. Inorg. Biochem.*, 2012, **114**, 38.
37 QikProp, *Version 2.5*, Schrödinger, LLC, New York, NY, 2005.
38 M. F. Snape, A. Misra, T. K. Murray, R. J. De Souza, J. L. Williams, A. J. Cross and A. R. Green, *Neuropharmacology*, 1999, **38**, 181.
39 J. C. Rochet, *Curr. Opin. Struct. Biol.*, 2000, **8**, 10.
40 D. M. Walsh, E. Thulin, A. M. Minogue, N. Gustavavsson, E. Pang, D. B. Teplow and S. Linse, *FEBS J.*, 2009, **276**, 1266.
41 H. Levine, *Protein Sci.*, 1993, **2**, 404.
42 M. Bartolini, C. Bertucci, M. L. Bolognesi, A. Cavalli, C. Melchiorre and V. Andrisano, *ChemBioChem*, 2007, **12**, 2152.
43 X. Chao, X. He, Y. Yang, X. Zhou, M. Jin, S. Liu, Z. Cheng, P. Liu, Y. Wang, J. Yu, Y. Tan, Y. Huang, J. Qin and S. Rapposelli, *Bioorg. Med. Chem. Lett.*, 2012, **22**, 6498.
44 S. Chaves, R. Jelic, C. Mendonça, M. Carrasco, Y. Yoshikawa, H. Sakurai and M. A. Santos, *Metallomics*, 2010, **2**, 220.
45 L. D. Devanur, H. Neubert and R. C. Hider, *J. Pharm. Sci.*, 2008, **97**, 1454.

46 M. Merkofer, A. Domazou, T. Nauser and W. H. Koppenol, *Eur. J. Inorg. Chem.*, 2006, 671.
47 W. L. F. Armarego and D. D. Perrin, *Purification of Laboratory Chemicals*, Butterworth-Heinemann, Oxford, 4th edn, 1999.
48 Maestro, *Version 7.5*, Schrödinger Inc., Portland, OR, 2005.
49 Macromodel, *Version 8.5*, Schrödinger Inc., Portland, OR, 1999.
50 J. Sebestík, S. M. Marques, P. L. Falé, S. Santos, D. M. Arduíno, S. M. Cardoso, C. R. Oliveira, M. L. Serralheiro and M. A. Santos, *J. Enzyme Inhib. Med. Chem.*, 2011, **26**, 485.
51 F. J. C. Rossotti and H. Rossotti, *J. Chem. Educ.*, 1965, **42**, 375.
52 P. Gans, A. Sabatini and A. Vacca, *Talanta*, 1996, **43**, 1739.
53 B. Tepe, O. Eminagaoglu, A. Akpulat and E. Aydin, *Food Chem.*, 2007, **100**, 985.
54 M. L. Michaelis, R. T. Dobrowsky and G. Li, *J. Mol. Neurosci.*, 2002, **19**, 289.
55 T. Mosmann, *J. Immunol. Methods*, 1983, **65**, 55.